Nonlinear effects in the Josephson-vortex terahertz photonic crystal: Second harmonic generation

A. Wall-Clarke and S. Savel'ev
Department of Physics, Loughborough University, Loughborough LE11 3TU, United Kingdom
(Received 20 April 2012; published 20 June 2012)

This paper considers nonlinear effects on the propagation of Josephson plasma waves in the Josephson-vortex photonic crystal in layered superconductors with the possibility of exciting the second harmonic, tunable by magnetic field. This would enable an increase in the operable frequency of THz superconducting devices such as generators, detectors, and filters. We demonstrate numerically that the second harmonic can be strongly amplified for certain resonance frequencies. The linear spectrum for the second harmonic has also been analyzed, finding the possible resonance points with the first harmonic spectrum. An analytical approach describing a spatial distribution of the THz Josephson plasma waves at and near the resonances is also developed.

DOI: 10.1103/PhysRevB.85.214521 PACS number(s): 74.25.Uv, 42.70.Qs

I. INTRODUCTION

Layered superconductors have been shown to be a useful system for the generation and control of THz radiation (see, e.g., reviews in Refs. 1–3). Consisting of a series of superconducting layers, separated by insulating barriers, these materials form a stack of Josephson junctions. Proposals have been made for the use of these materials as emitters,[4–15] detectors,[16–20] filters,[21–24] and other nonlinear and quantum devices[25–36] in the effort to bridge the THz gap. Recently, the main experimental obstacle in the way of THz superconducting electronics has been overcome. Coherent radiation above 1 μW has been produced[37–40] from a crystal of BSCCO up to 0.85 THz.

In order to control THz radiation in layered superconductors, Josephson vortices (JVs) can be used. For example, they allow the filtering of THz radiation via coherent scattering of propagating electromagnetic waves. Thus, a Josephson-vortex lattice formed in layered superconductors in an applied magnetic field can serve as a THz photonic crystal for Josephson plasma waves. Transparency of the THz photonic crystals can be controlled[21] by varying the applied magnetic field. Indeed, the spectrum of the JV photonic crystal shows band-gap structure as has been calculated.[24] The gaps in the Josephson plasma wave spectrum are tunable by an applied in-plane magnetic field H_{ab}. Namely, the JV lattice is created by the in-plane magnetic field H_{ab} parallel to the superconducting layers, and the distance between Josephson vortices can be readily changed by varying H_{ab}. JVs act as scattering centers for THz waves, forming a photonic band gap for frequencies in this range which are strongly reflected. The JV photonic crystal allows the propagation of waves above and near the Josephson plasma frequency ω_J, which has been shown to be within the THz range and tunable by magnetic field H_{ab} as well as the interlayer current $J_\perp$. Moreover, dynamics of JVs and THz Josephson plasma waves can be further controlled[41–44] by applying out-of-plane magnetic fields, which generate pancake vortices inside superconducting layers, which can attract JVs.

The dynamics of JVs and THz radiation (Josephson plasma waves) are governed by a coupled set of sine-Gordon equations describing the phase evolution of the superconducting order parameter in the material. The sine-Gordon equations have a nonlinearity due to the Josephson nonlinear relation between the superconducting current and electromagnetic fields. This nonlinearity[45] would affect the properties of the JV photonic crystals particularly when considering high-intensity radiation and/or frequency near the Josephson plasma frequency ω_J. Following the analogy with nonlinear optics,[46,47] a number of unusual effects can be expected in the nonlinear Josephson media. Materials with nonlinear refraction index have a response that varies according to the intensity of the electromagnetic waves in a nonlinear way. Unusual effects include higher harmonic generation, where the frequency of the input signal is increased by an integer factor, self-focusing of light, negative refractive index, sum-difference frequency mixing, among others. The nonlinearity of the sine-Gordon equation allows for the production of a second harmonic at double the input frequency if a strong enough in-plane field is applied. This would potentially increase the frequency range of THz radiation propagating through the JV photonic crystal if it could be understood how to excite this second harmonic. The main goal of this article is to show how to drive and control the second harmonic.

In Sec. II, the nonlinear equations for THz radiation in the JV photonic crystal are derived. We develop a perturbative approach to describe the generation of the second harmonic of THz radiation tunable by a magnetic field. In other words, we obtain solutions to these equations in terms of the first and second harmonics, leaving two coupled equations for the two harmonics only. In Sec. III, we solve these equations numerically and demonstrate that there are resonance frequencies where the second harmonic is strongly amplified. Section IV A discusses the linear spectrum of the second harmonic using Bloch wavelike solutions, comparing it to the first harmonic and finding possible resonance points between the two. In Sec. IV B, we propose an analytical approach to analyze the coupled equations for the first and second harmonics in JV photonic crystals and describe spatial distribution of the harmonics near the resonances.

II. DERIVING THE NONLINEAR EQUATIONS FOR FIRST AND SECOND HARMONICS

The structure of layered superconductors consists of thin superconducting layers (in the xz plane for the coordinate system used below) separated by normal barriers as shown in Fig. 1. JVs created by the applied magnetic field H_{ab} along

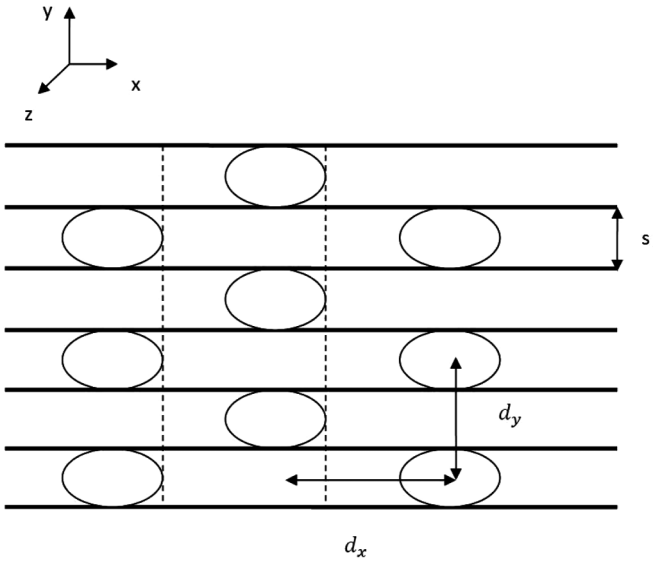

FIG. 1. Layered structure of the Josephson vortex photonic crystal, showing unit-cell boundaries on the x axis, and vortex cross sections along the z axis.

the z axis form a triangular lattice with a high anisotropy coefficient $\gamma = d_x/d_y$, where d_x and d_y are vortex spacings in the x and y directions, respectively (typical distance between layers is $s = 15$ Å, and anisotropy parameter is $\gamma = 300$–600; see, e.g., Ref. 48).

The spatial and temporal variance of the interlayer gauge-invariant phase difference φ of the order parameter for layered superconductors is given by the coupled sine-Gordon equations, which can be written in a continuous approximation as (see, e.g., Ref. 1)

$$\left[1-\lambda_{ab}^2\frac{\partial^2}{\partial y^2}\right]\left(\frac{1}{\omega_J^2}\frac{\partial^2\varphi}{\partial t^2}+\sin\varphi\right)-\lambda_c^2\frac{\partial^2\varphi}{\partial x^2}=0, \qquad (1)$$

where λ_c and λ_{ab} are the out-of-plane and in-plane London penetration depths, respectively. Here, we neglect the damping term, which is valid for samples thinner than the skin depth (about 0.3 mm for standard high-T_c superconductors). For larger samples, dissipation of Josephson plasma waves should be considered. However, the qualitative picture remains the same since the distance between vortices (the characteristic scale in Josephson-vortex photonic crystals) is much shorter than the characteristic damping scale for magnetic fields ($H \lesssim \Phi_0/\gamma s^2$) considered here. In other words, Josephson plasma waves scatter many times before they significantly decay if the temperature is low enough.

Representing φ as a sum of the solution φ_0 for JVs and the solution φ_1 for Josephson plasma waves (JPWs), we can write $\varphi = \varphi_0(x,y) + \varphi_1(x,y,t)$. Assuming $\varphi_1 \ll \varphi_0$, we can derive a perturbative algorithm for calculation of THz JPWs by expanding $\sin\varphi$ as $\sin\varphi \approx \sin\varphi_0 + (\cos\varphi_0)\varphi_1 - (\sin\varphi_0)\varphi_1^2/2$. In the following, we follow the approach developed in Ref. 24, thus, averaging Eq. (1) in the y direction (on the scale of the order of the distance between nearest JVs), we derive

$$\left[1-\lambda_{ab}^2\frac{\partial^2}{\partial y^2}\right]\left(\frac{1}{\omega_J^2}\frac{\partial^2\varphi_1}{\partial t^2}+\langle\cos\varphi_0\rangle\varphi_1+\frac{\langle\sin\varphi_0\rangle}{2}\varphi_1^2\right) - \lambda_c^2\frac{\partial^2\varphi_1}{\partial x^2}=0. \qquad (2)$$

Here, $\langle\sin\varphi_0\rangle$ and $\langle\cos\varphi_0\rangle$ are the average values of these functions across the layers. The form of these functions is discussed in Sec. III. So far,[21–24] only the linear properties of Eq. (2) have been discussed, ignoring the higher powers of φ_1. In order to analyze nonlinear properties of Josephson-vortex photonic crystals, these higher-order terms need to be taken into account.

After averaging along the y axis, the obtained equation (2) does not contain variables t and y explicitly. In other words, all coefficients are either constants or functions of the x variable only. This suggests an idea that we can try to find solution as a combination of waves $\psi_n\cos(n\omega t - nqy)$ with amplitudes varying along the x axis directed inside the crystal. Restricting ourselves with the first two terms in this combination, the solution of Eq. (2) can be written as $\varphi_1 = \psi_1(x)\cos(\omega t - qy) + \psi_2(x)\cos(2\omega t - 2qy)$. Substituting the last expression in (2) and ignoring all terms consisting of higher harmonics results in two coupled equations for the first and second harmonics:

$$(\langle\cos\varphi_0\rangle - \omega^2)\psi_1 - \frac{\lambda_c^2}{\left(1+\lambda_{ab}^2q^2\right)}\psi_1'' = \frac{\langle\sin\varphi_0\rangle}{2}\psi_1\psi_2, \qquad (3)$$

$$(\langle\cos\varphi_0\rangle - 4\omega^2)\psi_2 - \frac{\lambda_c^2}{\left(1+4\lambda_{ab}^2q^2\right)}\psi_2'' = \frac{\langle\sin\varphi_0\rangle}{4}\psi_1^2, \qquad (4)$$

where all frequencies are measured in units of ω_J.

Equations (3) and (4) are coupled, which allows for feedback between the first and second harmonics. Both equations take the form of a nonlinear Schrödinger equation in the amplitudes of the harmonics. Here, the "potential" term is described by $\cos\varphi_0(x)$. The second term in the left-hand side of Eqs. (3) and (4) can represent a kind of "effective mass" of Josephson plasma waves in the JV photonic crystal. Here, we would like to mention that our approach becomes incorrect for large $q \gtrsim 1/s$, i.e., for short wavelength along the y axis. In this short-wavelength limit, a discrete version of coupled sine-Gordon equations should be considered rather than their continuous limit.

III. NUMERICAL SIMULATIONS

A. Reducing to 1D problem

An approximate vortex solution of the sine-Gordon equations in a layer containing a JV is given by[49]

$$\varphi_0^v = \pi + 2\arctan\left(\frac{x}{l_0}\right). \qquad (5)$$

The phase change can be shown[24] to decay quickly away from the position of a JV both along and across junctions; this means that the phase φ_0 of the Josephson vortex lattice can be approximated as a sum of the phase φ_0^v of individual vortices. This is valid for moderate magnetic fields. It is useful to define

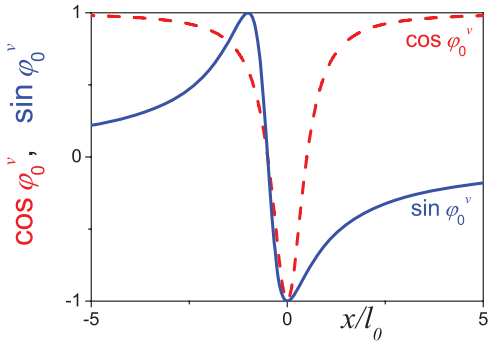

FIG. 2. (Color online) Graphs of $\cos\varphi_0^v(x)$ (which defines the effective potential in the equation for the first and second harmonics) and $\sin\varphi_0^v$ (which defines the interaction between the first and second harmonics) in the layer of a vortex. To plot these functions, Eqs. (8) and (10) were used.

a dimensionless magnetic field

$$h_{ab} = \frac{H_{ab}}{H_1} \tag{6}$$

given in terms of a characteristic field

$$H_1 = \frac{2\Phi_0}{\gamma s^2}, \tag{7}$$

where Φ_0 is the flux quantum. The above solution (5) for vortices is only valid for $h_{ab} \ll 1$.

Using (5), the value of $\cos\varphi_0^v$ (see Fig. 2) in the layer of a vortex can be given by[24]

$$\cos\varphi_0^v = -\frac{x^2 - l_o^2}{x^2 + l_o^2}. \tag{8}$$

By averaging $\cos\phi_0$ along the y axis, we finally derive

$$\langle\cos\varphi_0\rangle = -\frac{s}{d_y}\sum_n \frac{\left(x - \frac{2n+1}{2}d_x\right)^2 - l_o^2}{\left(x - \frac{2n+1}{2}d_x\right)^2 + l_o^2}. \tag{9}$$

In a similar way, function $\sin\varphi_0^v$ (see Fig. 2) in the vortex layer can be expressed as

$$\sin\varphi_0^v = -\frac{2l_o x}{x^2 + l_o^2}. \tag{10}$$

Averaging along the y axis results in the following equation:

$$\langle\sin\varphi_0\rangle = -\frac{s}{d_y}\sum_n \frac{2l_o\left(x - \frac{2n+1}{2}d_x\right)}{\left(x - \frac{2n+1}{2}d_x\right)^2 + l_o^2}. \tag{11}$$

Equations (3) and (4) together with effective $\langle\cos\varphi_0\rangle$ potential (9) and harmonic $\langle\sin\varphi_0\rangle$ interaction (11) fully describe propagation of the first and second harmonics of Josephson plasma waves through Josephson-vortex photonic crystals.

B. Numerical integration

In order to study the spatial distribution of the first and second harmonics described by the coupled equations (3) and (4), a simple numerical integration of these ordinary differential equations by using both Euler and higher-order multiderivative methods has been used. We numerically integrate these equations until the solution shows a "saturation behavior"

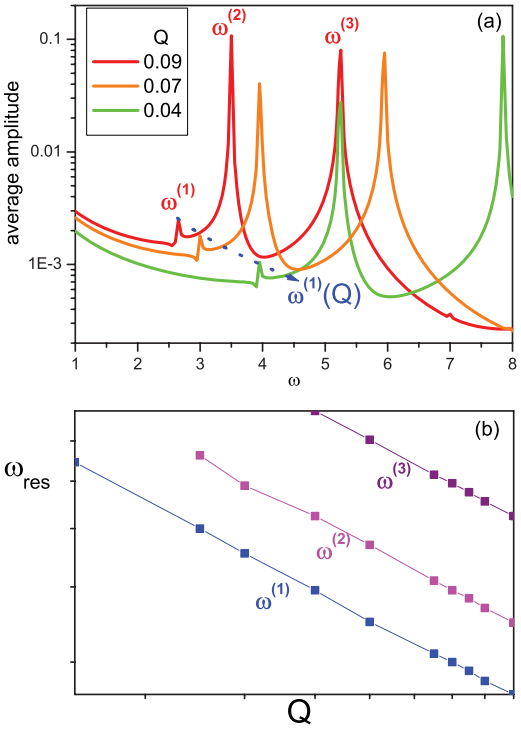

FIG. 3. (Color online) (a) Average second harmonic $\langle\psi_2^2\rangle$ as a function of frequency for $Q = d_x^2(1 + \lambda_{ab}^2 q^2)/\lambda_c^2$ shown in the plot, $l_o/d_x = 0.2$, $\psi_2(0) = \psi_2'(0) = 0$, $\psi_1(0) = 0.5$, $\psi_1'(0) = 0.2$, $\Delta x = 0.001$. Resonance frequencies are shown as $\omega^{(1)}$, $\omega^{(2)}$, $\omega^{(3)}$ near the corresponding resonance peaks. Blue arrow and blue symbol $\omega^{(1)}(Q)$ show the dependence of the resonance frequencies on Q. (b) Shift in resonance frequencies $\omega^{(1)}$, $\omega^{(2)}$, $\omega^{(3)}$ as a function of Q. All other parameters are the same as in (a).

and then measure the average value $\langle\psi_2^2\rangle$ [see Fig. 3(a)]. One can see sharp resonances where the second harmonic considerably enhances. Changing wave vector q along the y direction (i.e., changing JPW propagation direction) or varying the in-plane magnetic field h_{ab} results in variations in Q and in a shift in resonance frequencies [see Fig. 3(b)]. Thus, the resonance amplification (or optimal generation) of the second harmonic can be tuned by either the magnetic field or tilting the superconductor with respect to the incident THz radiation.

To understand the origin of the observed resonances, we plot a distribution of the second harmonic close and away from resonances (Fig. 4). Away from the resonance (blue curve in Fig. 4), the first harmonic generates a weak rather disordered oscillation indicating that the spatial periods (wavelengths) of these harmonics are not commensurate. In contrast, the spatial oscillations of the second harmonic near the resonance are very regular and the amplitude of the oscillation increases at the resonance (black curve in Fig. 4). When analyzing the envelope curve (inset in Fig. 4) at larger distances, we observe that the second harmonic amplitude oscillates with a quite large period. Finally, we conclude that these resonances occur under certain matching conditions for the spatial periods of the first and the second harmonics. Therefore, in order to develop an analytical approach of the second harmonic enhancement in THz Josephson-vortex photonic crystals, one

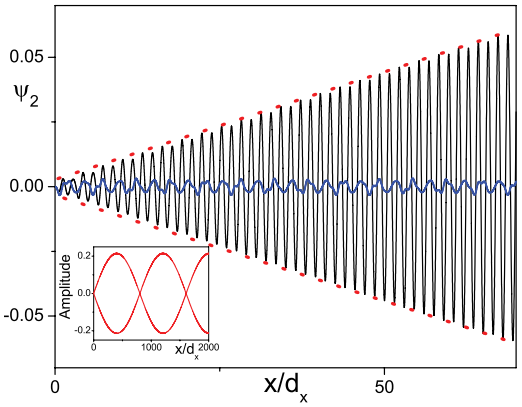

FIG. 4. (Color online) Spatial distribution $\psi_2(x)$ of the second harmonic near $\omega = 3.5$ (black line) and away from $\omega = 2$ (blue line) the resonance $\omega^{(1)}$ for $Q = 0.09$. The regular oscillation with increasing amplitude is clearly seen near the resonance. By plotting the amplitude of the oscillations (shown by red dashed curve in the main panel), we observe oscillation of the second harmonic amplitude at larger scales (see inset).

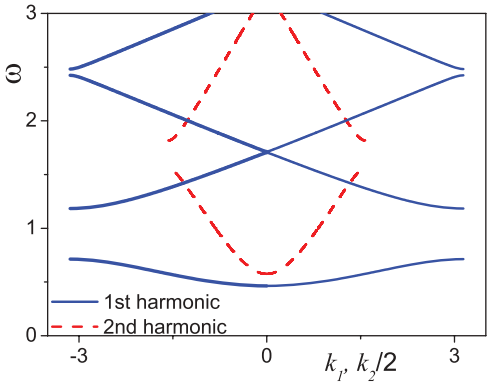

FIG. 5. (Color online) Comparison of spectrum of JPWs for the first harmonic $\omega(k_1)$ (shown in blue) and the second $\omega(k_2/2)$ harmonic (shown in green) for the case $h_{ab} = 0.2$, $qs = 0.3\pi$ (when $k_{1,2}$ is normalized by $1/d_x$). To calculate these spectra, we use Eq. (14) with $\alpha_{1,2}$ and $\beta_{1,2}$ calculated for the first and second harmonics by using Eqs. (15) and (16). The spectrum for the second harmonic shown as a function of $k_2/2$ rather than k_2 in order to locate resonances $\omega(k_1) = \omega(k_2/2)$ discussed below.

needs to consider cases when wavelengths of these harmonics are commensurate.

IV. SOLVING THE NONLINEAR EQUATIONS

A. Linear spectra for the first and second harmonics

The linear spectrum for the first harmonic propagating through Josephson-vortex photonic crystals has been obtained in Ref. 24 by solving Eq. (3) with no second harmonic ($\psi_2 = 0$) and by seeking solution in the form of Bloch waves:

$$\psi_{L1} = u_{L1}(x)e^{ik_1 x} \tag{12}$$

Here, k_1 is the quasi-wave-vector of the first harmonic located within the first Brillouin zone ($-\pi/d_x < k_1 < \pi/d_x$), the Bloch wave amplitude $u_{L1}(x)$ is a periodic function with period d_x [i.e., $u_{L1}(x + d_x) = u_{L1}(x)$], while subindex "1" refers to the first harmonic. In this section, we compare linear spectra for the first and the second harmonics with a goal to locate possible harmonic matching conditions. Using stepwise approximation (see for detail Ref. 24) of $\langle \cos \phi_0^v \rangle$, we can derive spectra for both the first and second harmonics analytically. Indeed, the linear spectrum for the second harmonic can be obtained in the same way as for the first harmonic by ignoring the nonlinear right-hand side of Eq. (4), then using a Bloch wave solution of the form

$$\psi_{L2} = u_{L2}(x)e^{ik_2 x} \tag{13}$$

for the linear part of Eq. (4) with zero right-hand side. Here, a periodic function $u_{L2}(x + d_x) = u_{L2}(x)$ is the Bloch wave amplitude, the quasi-wave-vector k_2 is located in $-\pi/d_x < k_2 < \pi/d_x$, and subindex "2" refers to the second harmonic. Applying periodic boundary conditions of the period of the unit cell of the vortex lattice allows the spectrum to be derived as follows:

$$\cos(kd_x) = \cos\alpha l_1 \cos\beta l_2 - \frac{\alpha^2 + \beta^2}{2\alpha\beta} \sin\alpha\, l_1 \sin\beta l_2. \tag{14}$$

Here, α and β take different values for the first and second harmonics:

$$\alpha_n = k_0(q)\sqrt{n^2\omega^2 - 1}, \quad \beta_n = k_0(q)\sqrt{n^2\omega^2 + \pi\sqrt{h_{ab} - 1}}, \tag{15}$$

although the overall structure of both spectra remains the same. Here, subindex n takes 1 or 2 and refers to the first harmonic or the second harmonic, respectively, while k_0 is defined by the following expression:

$$k_0^2 = \frac{1 + n^2\lambda_{ab}^2 q^2}{\lambda_c^2}. \tag{16}$$

The spectrum for the second harmonic as shown in Fig. 5 is very similar to the first harmonic and displays similar photonic band gaps. The position of these band gaps is directly proportional to the applied magnetic field. As we see in the following, the matching condition for the first and the second harmonics is $k_2 = 2k_1$. Therefore, we plot $\omega(k_1)$ and $\omega(k_2/2)$ in order to locate the resonance points.

B. Resonance approximation for the harmonics

In the attempt to find analytical solutions to Eqs. (3) and (4), it can be assumed that the nonlinearity is weak and defines slowly varying harmonic amplitudes $A_{1,2}$, which change over a much larger scale than the vortex-lattice period. This approach has been successfully used for the analysis of optical nonlinear photonic crystals.[50] Here, we plan to apply this method for our two harmonic Josephson plasma waves propagating through Josephson-vortex THz photonic crystals. Following the approach in Ref. 50, we have to introduce the first and the second harmonic amplitudes A_1 and A_2:

$$\psi_1 = A_1\Psi_{L1}, \quad \psi_2 = A_2\Psi_{L2}, \tag{17}$$

where the subindices refer to the first and the second harmonics, respectively. Here, we assume that A_1 and A_2 are slowly varying amplitudes of $\Psi_{L1} = \mathrm{Re}(\psi_{L1})$ and $\Psi_{L2} = \mathrm{Re}(\psi_{L2})$,

which are the solutions of the linear part of Eqs. (3) and (4) (i.e., solutions without the nonlinear terms in the right-hand side). To solve *nonlinear* equations (3) and (4), we have to replace complex representation of Bloch waves $\psi_{L1} = u_{L1}e^{ik_1x}$ and $\psi_{L2} = u_{L2}e^{ik_2x}$ by their real parts (representing the real function solution of the same equations) as follows:

$$\begin{aligned}\Psi_{L1} &= \mathrm{Re}(\psi_{L1}) = u_1 \cos k_1 x - v_1 \sin k_1 x,\\ \Psi_{L2} &= \mathrm{Re}(\psi_{L2}) = u_2 \cos k_2 x - v_2 \sin k_2 x,\end{aligned} \tag{18}$$

where $u_1 = \mathrm{Re}(u_{1L})$, $v_1 = \mathrm{Im}(u_{1L})$ and $u_2 = \mathrm{Re}(u_{2L})$, $v_2 = \mathrm{Im}(u_{2L})$. This should be done due to problems arising when using the complex wave solutions in the nonlinear equations (3) and (4). The real functions $u_{1,2}$ and $v_{1,2}$ are periodic with one cell period, while functions $\cos(k_1x)$, $\sin(k_1x)$ and $\cos(k_2x)$, $\sin(k_2x)$ are periodic with the period of the wavelengths $\lambda_1 = 2\pi/k_1$ and $\lambda_2 = 2\pi/k_2$ of the first and the second harmonics, respectively. In order to simplify calculations below, we assume that $|A_{1,2}|/|dA_{1,2}/dx| \gg \lambda_{1,2} \gg d_x$.

Substituting Eqs. (17) and (18) into (3) and (4), two equations for the nonlinear amplitudes can be obtained:

$$\Psi_{L1}^{'}A_1^{'} = -\frac{q^2}{\gamma^2}\frac{\langle \sin\varphi_0\rangle}{2}\Psi_{L1}\Psi_{L2}A_1A_2, \tag{19}$$

$$\Psi_{L2}^{'}A_2^{'} = -\frac{q^2}{\gamma^2}\langle \sin\varphi_0\rangle \Psi_{L1}^2A_1^2, \tag{20}$$

where we neglect terms that are proportional to $A_{1,2}^{''}$. Now, we have to notice that there are three different spatial scales in this problem. The shortest one is the size d_x of the Josephson THz photonic crystal cell. If considering the wave vectors $k_{1,2}$ of the first and the second harmonics to be not very close to the Brillouin zone boundary $\pm\pi/d_x$, then the wavelengths of these harmonics are much larger than the cell size d_x, but they are still much smaller than the characteristic scale $|A_{1,2}|/|dA_{1,2}/dx|$ of variations of the harmonic amplitudes if nonlinearity is weak enough. So, we can average Eqs. (19) and (20) in two stages: First, we can average Eqs. (19) and (20) within the photonic crystal cell (on scales d_x) by assuming that both $A_{1,2}$ as well as $\cos k_{1,2}x$ and $\sin k_{1,2}x$ are slow functions; then, we can average once more over $\cos k_{1,2}x$ and $\sin k_{1,2}x$ by assuming that only $A_{1,2}$ are slow. Following this procedure (see Appendix), we derive equations for amplitudes which are valid in resonance points $k_2 = 2k_1$:

$$A_1^{'} = I_1A_1A_2, \tag{21}$$

$$A_2^{'} = I_2A_1^2, \tag{22}$$

where I_1 and I_2 are not functions of x and are defined by the integrals

$$\begin{aligned}I_1 &= -\frac{q^2\int_0^L dx\langle\sin\varphi_0\rangle[\mu_1(u_1u_2+v_1v_2)+\eta_1(u_1v_2-v_1u_2)]}{4\gamma^2\int_0^L dx\left(\mu_1^2+\eta_1^2\right)},\\ I_2 &= -\frac{q^2\int_0^L dx\langle\sin\varphi_0\rangle\left[\mu_2\left(u_1^2-v_1^2\right)+2\eta_2u_1v_1\right]}{2\gamma^2\int_0^L dx\left(\mu_2^2+\eta_2^2\right)}\end{aligned} \tag{23}$$

with $\mu_j = u_j^{'} - k_jv_j$, $\eta_j = v_j^{'} + k_ju_j$, and $j = 1$ or 2.

Since I_1 and I_2 are constants, we can analytically calculate the distribution of the harmonic amplitudes. By dividing Eq. (21) by (22) and separating A_1 and A_2, an integrable expression can be obtained:

$$A_1A_1^{'} = \frac{I_1}{I_2}A_2A_2^{'}. \tag{24}$$

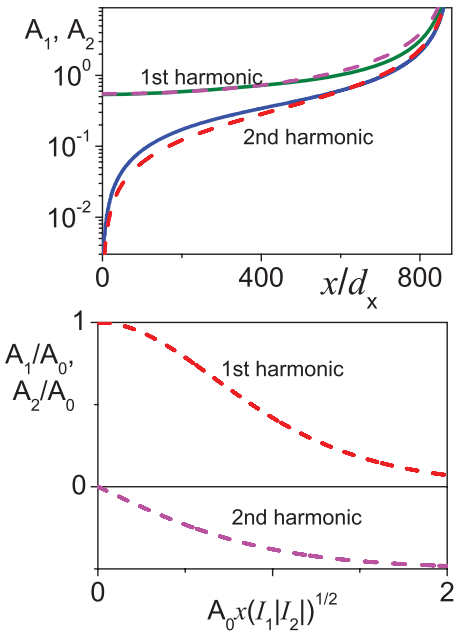

FIG. 6. (Color online) (a) Harmonic amplitudes versus normalized distance x/d_x from the sample surface. Solid curves were obtained by simulations of coupled equations (3) and (4) for the first and the second harmonics at $\omega = 3.49$ and other parameters to be the same as in Fig. 4. Dashed curve is the solution in the resonance approximations (27) and (28) for $\sqrt{I_1I_2} = 0.0036$ and $\sqrt{I_2/I_1} = 0.65$. (b) Harmonic amplitudes distribution for the second type of the resonance described by Eqs. (29) and (30) with $\sqrt{I_2/I_1} = 0.5$.

In order to integrate this expression, we have to use boundary conditions: the second harmonic is zero $A_2(0) = 0$ at the sample boundary ($x = 0$) since we assume that it is generated by the first harmonic in the sample rather than coming from the vacuum, while $A_1(0) = A_0$. In other words, the first harmonic amplitude is set to A_0 and the second harmonic amplitude is set to zero at the vacuum-crystal interface. By integrating Eq. (24), we derive an expression linking A_1 and A_2 as follows:

$$A_1^2 = \frac{I_1}{I_2}A_2^2 + A_0^2. \tag{25}$$

Equations (21) and (22) can now be decoupled using Eq. (25), resulting in

$$A_2^{'} = I_1A_2^2 + I_2A_0^2. \tag{26}$$

The form of the solutions, though, depends strongly on the signs of the integrals I_1 and I_2. When integrals have the same signs (e.g., $I_1 > 0$, $I_2 > 0$), the solutions for the first and second harmonic amplitudes can be written as

$$A_1(x) = A_0\sec(A_0\sqrt{I_1I_2}x), \tag{27}$$

$$A_2(x) = A_0\sqrt{\frac{I_2}{I_1}}\tan(A_0\sqrt{I_1I_2}x). \tag{28}$$

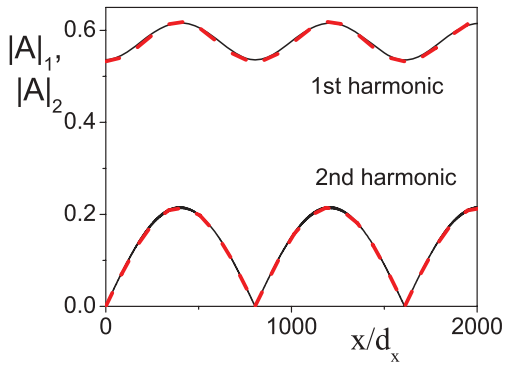

FIG. 7. (Color online) Harmonic amplitudes versus normalized distance x/d_x from the sample surface. Solid curves were obtained by simulations of coupled equations (3) and (4) for the first and the second harmonics at $\omega = 3.5$ (i.e., near the resonance) and other parameters to be the same as in Fig. 4. Dashed curve is the solution in the near-resonance approximations (33) and (34) for $\sqrt{\tilde{I}_1\tilde{I}_2}/\delta k = 0.015$, $\sqrt{\tilde{I}_2/\tilde{I}_1} = 56$, $\alpha = 0$, and $\delta k = 0.004$.

These solutions [called type-I resonance, Fig. 6(a)] diverge at distance $x = \pi/(2A_0\sqrt{I_1 I_2})$. For the case when I_2 and I_1 have different signs (e.g., $I_2 < 0$, $I_1 > 0$), the solutions [type-II resonance, Fig. 6(b)] have no singularities:

$$A_1(x) = A_0 \mathrm{sech}(A_0\sqrt{I_1|I_2|}x), \tag{29}$$

$$A_2(x) = -A_0\sqrt{\frac{|I_2|}{I_1}}\tanh(A_0\sqrt{I_1|I_2|}x). \tag{30}$$

By varying frequency near the resonance $\omega^{(2)}$ in our simulations of Eqs. (3) and (4), we observe the divergence of $\langle\psi_2^2\rangle$ at $\omega = 3.49$, indicating that we have type-I resonance point. An attempt to fit the simulations by our analytical formulas (27) and (28) results in a quite good quantitative agreement [Fig. 6(a), solid versus dashed curves].

For frequencies close (but not exactly satisfying) to the resonance conditions (i.e., $\delta k = 2k_1 - k_2$, $|\delta k| \ll k_2$), we derive (see Appendix) the following set of equations:

$$A_1' = \tilde{I}_1 A_1 A_2 \cos(\delta k x + \alpha_1), \tag{31}$$

$$A_2' = \tilde{I}_2 A_1^2 \cos(\delta k x + \alpha_2) \tag{32}$$

with constants $\tilde{I}_{1,2}$ and $\alpha_{1,2}$. If $\alpha_1 = \alpha_2$, this equation can be easily solved. For instance, for $\alpha = 0$ we can write the following solutions:

$$A_1(x) = A_0 \sec(A_0\sqrt{\tilde{I}_1\tilde{I}_2}\sin(\delta k x)/\delta k), \tag{33}$$

$$A_2(x) = A_0\sqrt{\frac{\tilde{I}_2}{\tilde{I}_1}}\tan(A_0\sqrt{\tilde{I}_1\tilde{I}_2}\sin(\delta k x)/\delta k) \tag{34}$$

for $\tilde{I}_{1,2}\cos(\alpha_{1,2}) > 0$. These solutions can be used to fit (Fig. 7) amplitude oscillations obtained in our simulations (see inset in Fig. 4). A good fit (Fig. 7, dashed versus solid curves) of our analytical and numerical results shows that a generalization of the usual method describing nonlinear photonic crystal (Ref. 50) allows us to quite accurately describe the generation of second harmonic near the matching resonances in Josephson-vortex THz photonic crystals.

V. CONCLUSIONS

The above simulations and analytical calculations suggest that the second harmonic can be generated in the Josephson-vortex photonic crystal within certain frequency ranges with an amplitude that depends strongly on frequency. These second harmonics can be strongly enhanced at resonances which depend on the vortex-lattice period controlled by applied magnetic field. The analytical approach proposed here quite accurately describes the distribution of the first and second harmonics near the resonances and suggests two different types of the possible resonance points.

We would like to stress that the Josephson-vortex photonic crystal allows more efficient control of the generation of high harmonics of Josephson plasma waves. First of all, even harmonics (including the second harmonic) can not be created in a vortex-free sample due to the oddlike nonlinearity of the sine-Gordon equation. Also, due to a band-gap structure of THz Josephson plasma waves in Josephson photonic crystals, multiple resonances occur when the linear spectra of the first and the second harmonics of Josephson plasma waves cross, which is not the case for vortex-free samples. These resonances can be tuned by in-plane magnetic field, which allows considerable enhancement of the second harmonic of any desirable frequency, so we propose a nonlinear higher-harmonic THz generator tunable by an applied magnetic field.

APPENDIX: EQUATIONS FOR HARMONIC AMPLITUDES

Multiplying Eqs. (19) by Ψ_{L1}' and (20) by Ψ_{L2}' and averaging over one Josephson THz photonic cell, we derive

$$\begin{aligned}&(Y_{1,1}\cos^2 k_1 x - 2Y_{1,2}\cos k_1 x \sin k_1 x + Y_{1,3}\sin^2 k_1 x)A_1' \\ &= -\frac{q^2}{2\gamma^2}A_1 A_2(Z_{1,1}\cos^2 k_1 x\cos k_2 x - Z_{1,2}\cos k_1 x \sin k_1 x \cos k_2 x + Z_{1,3}\sin^2 k_1 x \cos k_2 x \\ &\quad - Z_{1,4}\cos^2 k_1 x \sin k_2 x + Z_{1,5}\sin k_1 x \cos k_1 x \sin k_2 x - Z_{1,6}\sin^2 k_1 x \sin k_2 x),\end{aligned} \tag{A1}$$

$$\begin{aligned}&(Y_{2,1}\cos^2 k_2 x - 2Y_{2,2}\cos k_2 x \sin k_2 x + Y_{2,3}\sin^2 k_2 x)A_1' \\ &= -\frac{q^2}{\gamma^2}A_1^2(Z_{2,1}\cos^2 k_1 x\cos k_2 x - Z_{2,2}\cos k_1 x \sin k_1 x \cos k_2 x + Z_{2,3}\sin^2 k_1 x \cos k_2 x \\ &\quad - Z_{2,4}\cos^2 k_1 x \sin k_2 x + Z_{2,5}\cos k_1 x \sin k_1 x \sin k_2 x - Z_{2,6}\sin^2 k_1 x \sin k_2 x),\end{aligned} \tag{A2}$$

where

$$Y_{j,1} = \frac{1}{L}\int_0^L (u_j' - v_j k_j)^2 dx,$$
$$Y_{j,2} = \frac{1}{L}\int_0^L (u_j' - v_j k_j)(v_j' + k_j u_j) dx,$$
$$Y_{j,3} = \frac{1}{L}\int_0^L (v_j' + k_j u_j)^2 dx,$$
$$Z_{1,1} = \frac{1}{L}\int_0^L \langle \sin\varphi_0\rangle (u_1' - v_1 k_1) u_1 u_2 dx,$$
$$Z_{1,2} = \frac{1}{L}\int_0^L \langle \sin\varphi_0\rangle [(u_1' - k_1 v_1) v_1 u_2 + (v_1' + k_1 u_1) u_1 u_2] dx,$$
$$Z_{1,3} = \frac{1}{L}\int_0^L \langle \sin\varphi_0\rangle (v_1' + k_1 u_1) v_1 u_2 dx,$$
$$Z_{1,4} = \frac{1}{L}\int_0^L \langle \sin\varphi_0\rangle (u_1' - k_1 v_1) u_1 v_2 dx,$$
$$Z_{1,5} = \frac{1}{L}\int_0^L \langle \sin\varphi_0\rangle [(u_1' - k_1 v_1) v_1 v_2 + (v_1' + k_1 u_1) u_1 v_2] dx,$$
$$Z_{1,6} = \frac{1}{L}\int_0^L \langle \sin\varphi_0\rangle (v_1' + k_1 u_1) v_1 v_2 dx,$$
$$Z_{2,1} = \frac{1}{L}\int_0^L \langle \sin\varphi_0\rangle (u_2' - v_2 k_2) u_1^2 dx,$$
$$Z_{2,2} = \frac{2}{L}\int_0^L \langle \sin\varphi_0\rangle (u_2' - k_2 v_2) u_1 v_1] dx,$$
$$Z_{2,3} = \frac{1}{L}\int_0^L \langle \sin\varphi_0\rangle (u_2' - k_2 v_2) v_1^2 dx,$$
$$Z_{2,4} = \frac{1}{L}\int_0^L \langle \sin\varphi_0\rangle (v_2' + k_2 u_2) u_1^2 dx,$$
$$Z_{2,5} = \frac{2}{L}\int_0^L \langle \sin\varphi_0\rangle (v_2' + k_2 u_2) v_1 u_1 dx,$$
$$Z_{2,6} = \frac{1}{L}\int_0^L \langle \sin\varphi_0\rangle (v_2' + k_2 u_2) v_1^2 dx.$$

Now, we can assume that the amplitudes A_1 and A_2 vary slowly also on scales of the order of the wavelength of the first and the second harmonics, thus we can also average the derived equations on the scale of $\mathcal{L} > \max(2\pi/k_1, 2\pi/k_2)$. Due to fast oscillations of $\cos k_{1,2}x$ and $\sin k_{1,2}x$, this averaging results in trivial equations $A_1' = A_3' = 0$ for all k_1 and k_2 apart of resonance points $k_2 = 2k_1$ where the coupling of the first and the second harmonics are most efficient. In the resonance point $k_2 = 2k_1$, we obtain

$$\left(\frac{Y_{1,1}}{2} + \frac{Y_{1,3}}{2}\right) A_1' = -\frac{q^2}{2\gamma^2} A_1 A_2 \left(\frac{Z_{1,1}}{4} - \frac{Z_{1,3}}{4} + \frac{Z_{1,5}}{4}\right), \tag{A3}$$

$$\left(\frac{Y_{2,1}}{2} + \frac{Y_{2,3}}{2}\right) A_1' = -\frac{q^2}{\gamma^2} A_1^2 \left(\frac{Z_{2,1}}{4} - \frac{Z_{2,3}}{4} + \frac{Z_{2,5}}{4}\right). \tag{A4}$$

The approach discussed above also allows analyzing spatial distribution of harmonics near the resonance $\delta k = 2k_1 - k_2$, $|\delta k|/k_2 \ll 1$. In this case, we have to assume that oscillations $\cos \delta k x$ and $\sin \delta k x$ are slow and keep the corresponding terms in (A1) and (A2). All other spatial oscillations can be averaged out. As a result, we derive

$$(Y_{1,1} + Y_{1,3}) A_1' = -\frac{q^2}{4\gamma^2} A_1 A_2 [(Z_{1,1} - Z_{1,3} + Z_{1,5}) \cos \delta k x + (-Z_{1,2} + Z_{1,4} + Z_{1,6}) \sin \delta k x], \tag{A5}$$

$$(Y_{2,1} + Y_{2,3}) A_1' = -\frac{q^2}{2\gamma^2} A_1 A_2 [(Z_{2,1} - Z_{2,3} + Z_{2,5}) \cos \delta k x + (-Z_{2,2} + Z_{2,4} + Z_{2,6}) \sin \delta k x]. \tag{A6}$$

The above equations can be easily rewritten in the form presented in the main text.

[1] S. Savel'ev, V. A. Yampol'skii, A. L. Rakhmanov, and F. Nori, Rep. Prog. Phys. **73**, 026501 (2010).
[2] X. Hu and S. Z. Lin, Supercond. Sci. Technol. **23**, 053001 (2010).
[3] V. P. Koshelets and S. V. Shitov, Supercond. Sci. Technol. **13**, R53 (2000).
[4] M. Tachiki, M. Iizuka, K. Minami, S. Tejima, and H. Nakamura, Phys. Rev. B **71**, 134515 (2005).
[5] S. Savel'ev, V. Yampol'skii, A. Rakhmanov, and F. Nori, Phys. Rev. B **72**, 144515 (2005); Phys. C (Amsterdam) **437–438**, 281 (2006); **445**, 175 (2006).
[6] A. L. Rakhmanov, S. E. Savel'ev, and F. Nori, Phys. Rev. B **79**, 184504 (2009).
[7] F. Marchesoni, S. Savel'ev, M. Tachiki, and F. Nori, Phys. Rev. B **81**, 174531 (2010).
[8] W. Zhou, C. Wang, and Q.-H. Chen, Phys. Rev. B **82**, 184514 (2010).
[9] A. E. Koshelev, Phys. Rev. B **82**, 174512 (2010).
[10] I. Martin, Gábor B. Halász, L. N. Bulaevskii, and A. E. Koshelev, J. Appl. Phys. **108**, 033908 (2010).
[11] M. Tachiki, S. Fukuya, and T. Koyama, Phys. Rev. Lett. **102**, 127002 (2009).
[12] T. Koyama, H. Matsumoto, M. Machida, and K. Kadowaki, Phys. Rev. B **79**, 104522 (2009).
[13] A. E. Koshelev and L. N. Bulaevskii, Phys. Rev. B **77**, 014530 (2008).
[14] L. N. Bulaevskii and A. E. Koshelev, Phys. Rev. Lett. **99**, 057002 (2007).
[15] M. Tachiki, K. Ivanovic, K. Kadowaki, and T. Koyama, Phys. Rev. B **83**, 014508 (2011).
[16] S. Savel'ev, V. Yampol'skii, and F. Nori, Phys. Rev. Lett. **95**, 187002 (2005); Phys. C (Amsterdam) **445**, 183 (2006).
[17] S. Savel'ev, V. A. Yampol'skii, A. L. Rakhmanov, and F. Nori, Phys. Rev. B **75**, 184503 (2007).
[18] V. A. Yampol'skii, A. V. Kats, M. L. Nesterov, A. Yu. Nikitin, T. M. Slipchenko, S. Savel'ev, and F. Nori, Phys. Rev. B **76**, 224504 (2007); **79**, 214501 (2009).
[19] V. A. Yampol'skii, D. R. Gulevich, Sergey Savel'ev, and Franco Nori, Phys. Rev. B **78**, 054502 (2008).

[20]D. V. Kadygrob, V. A. Golick, V. A. Yampol'skii, T. M. Slipchenko, D. R. Gulevich, and S. Savel'ev, Phys. Rev. B **80**, 184512 (2009).
[21]S. Savel'ev, A. L. Rakhmanov, and F. Nori, Phys. Rev. Lett. **94**, 157004 (2005); Phys. C (Amsterdam) **445**, 180 (2006).
[22]H. Susanto, E. Goldobin, D. Koelle, R. Kleiner, and S. A. van Gils, Phys. Rev. B **71**, 174510 (2005).
[23]V. A. Yampol'skii, Sergey Savel'ev, O. V. Usatenko, S. S. Mel'nik, F. V. Kusmartsev, A. A. Krokhin, and Franco Nori, Phys. Rev. B **75**, 014527 (2007).
[24]S. Savel'ev, A. L. Rakhmanov, and F. Nori, Phys. Rev. B **74**, 184512 (2006).
[25]V. A. Yampol'skii, S. Savel'ev, A. L. Rakhmanov, and F. Nori, Phys. Rev. B **78**, 024511 (2008).
[26]V. A. Yampol'skii, T. M. Slipchenko, Z. A. Mayzelis, D. V. Kadygrob, S. S. Apostolov, S. E. Savel'ev, and F. Nori, Phys. Rev. B **78**, 184504 (2008).
[27]S. Savel'ev, A. L. Rakhmanov, and F. Nori, Phys. Rev. Lett. **98**, 077002 (2007); **98**, 269901(E) (2007).
[28]S. Savel'ev, A. L. Rakhmanov, X. Hu, A. Kasumov, and F. Nori, Phys. Rev. B **75**, 165417 (2007).
[29]S. Savel'ev, A. O. Sboychakov, A. L. Rakhmanov, and F. Nori, Phys. Rev. B **77**, 014509 (2008).
[30]A. O. Sboychakov, S. Savel'ev, A. L. Rakhmanov, and F. Nori, Europhys. Lett. **80**, 17009 (2007).
[31]A. O. Sboychakov, Sergey Savel'ev, A. L. Rakhmanov, and Franco Nori, Phys. Rev. Lett. **104**, 190602 (2010).
[32]B. Chesca, S. E. Savel'ev, A. L. Rakhmanov, H. J. H. Smilde, and H. Hilgenkamp, Phys. Rev. B **78**, 094505 (2008).
[33]A. L. Rakhmanov, A. M. Zagoskin, Sergey Savel'ev, and Franco Nori, Phys. Rev. B **77**, 144507 (2008).
[34]D. R. Gulevich, F. V. Kusmartsev, S. Savel'ev, V. A. Yampol'skii, and F. Nori, Phys. Rev. Lett. **101**, 127002 (2008).
[35]D. R. Gulevich, F. V. Kusmartsev, S. Savel'ev, V. A. Yampol'skii, and F. Nori, Phys. Rev. B **80**, 094509 (2009).
[36]D. R. Gulevich, S. Savel'ev, V. A. Yampol'skii, F. V. Kusmartsev, and F. Nori, J. Appl. Phys. **104**, 064507 (2008).
[37]L. Ozyuzer, A. E. Koshelev, C. Kurter, N. Gopalsami, Q. Li, M. Tachiki, K. Kadowaki, T. Yamamoto, H. Minami, H. Yamaguchi, T. Tachiki, K. E. Gray, W. K. Kwok, and U. Welp, Science **318**, 1291 (2007).
[38]K. Kadowaki, H. Yamaguchi, K. Kawamata, T. Yamamoto, H. Minami, I. Kakeya, U. Welp, L. Ozyuzer, A. Koshelev, C. Kurter, K. E. Gray, and W. K. Kwok, Phys. C (Amsterdam) **468**, 634 (2008).
[39]H. Minami, I. Kakeya, H. Yamaguchi, T. Yamamoto, and K. Kadowaki, Appl. Phys. Lett. **95**, 232511 (2009).
[40]M. Tsujimoto, K. Yamaki, K. Deguchi, T. Yamamoto, T. Kashiwagi, H. Minami, M. Tachiki, K. Kadowaki, and R. A. Klemm, Phys. Rev. Lett. **105**, 037005 (2010).
[41]A. E. Koshelev, Phys. Rev. Lett. **83**, 187 (1999).
[42]S. E. Savel'ev, J. Mirković, and K. Kadowaki, Phys. Rev. B **64**, 094521 (2001).
[43]S. Savel'ev and F. Nori, Nat. Mater. **1**, 179 (2002).
[44]D. Cole *et al.*, Nat. Mater. **5**, 305 (2006).
[45]S. Savel'ev, A. Rakhmanov, V. Yampol'skii, and F. Nori, Nat. Phys. **2**, 521 (2006).
[46]D. C. Mills, *Nonlinear Optics* (Springer, Berlin, 1998).
[47]R. W. Boyd, *Nonlinear Optics* (Academic, New York, 2003).
[48]J. Mirković, S. E. Savel'ev, E. Sugahara, and K. Kadowaki, Phys. Rev. Lett. **86**, 886 (2001).
[49]A. Gurevich, Phys. Rev. B **46**, R3187 (1992).
[50]M. Bertolotti, J. Opt. A **8**, S9 (2006).